




Article

Dual X-ray- and Neutron-Shielding Properties of Gd₂O₃/NR Composites with Autonomous Self-Healing Capabilities

Worawat Poltabtim^{1,2,3} , Arkarapol Thumwong^{3,4}, Ekachai Wimolmala⁵, Chanis Rattanapongs^{1,3}, Shinji Tokonami² , Tetsuo Ishikawa⁶ and Kiadtisak Saenboonruang^{1,3,7,8,*} 

¹ Department of Applied Radiation and Isotopes, Faculty of Science, Kasetsart University, Bangkok 10900, Thailand

² Institute of Radiation Emergency Medicine, Hirosaki University, Aomori 0368564, Japan

³ Special Research Unit of Radiation Technology for Advanced Materials (RTAM), Faculty of Science, Kasetsart University, Bangkok 10900, Thailand

⁴ Department of Materials Science, Faculty of Science, Kasetsart University, Bangkok 10900, Thailand

⁵ Polymer Processing and Flow (P-PROF) Research Group, Division of Materials Technology, School of Energy, Environment and Materials, King Mongkut's University of Technology Thonburi, Bangkok 10140, Thailand

⁶ Department of Radiation Physics and Chemistry, Fukushima Medical University, Fukushima 9601295, Hikarigaoka, Japan

⁷ Kasetsart University Research and Development Institute (KURDI), Kasetsart University, Bangkok 10900, Thailand

⁸ Specialized Center of Rubber and Polymer Materials in Agriculture and Industry (RPM), Faculty of Science, Kasetsart University, Bangkok 10900, Thailand

* Correspondence: kiadtisak.s@ku.th; Tel.: +66-2-562-5555 (ext. 646219)

Abstract: The neutron- and X-ray-shielding, morphological, physical, mechanical, and self-healing properties were investigated for natural rubber (NR) composites containing varying gadolinium oxide (Gd₂O₃) contents (0, 25, 50, 75, and 100 parts per hundred parts of rubber; phr) to investigate their potential uses as self-healing and flexible neutron- and X-ray-shielding materials. Gd₂O₃ was selected as a radiation protective filler in this work due to its preferable properties of having relatively high neutron absorption cross-section (σ_{abs}), atomic number (Z), and density (ρ) that could potentially enhance interaction probabilities with incident radiation. The results indicated that the overall neutron-shielding and X-ray-shielding properties of the NR composites were enhanced with the addition of Gd₂O₃, as evidenced by considerable reductions in the half-value layer (HVL) values of the samples containing 100 phr Gd₂O₃ to just 1.9 mm and 1.3 mm for thermal neutrons and 60 kV X-rays, respectively. Furthermore, the results revealed that, with the increase in Gd₂O₃ content, the mean values (\pm standard deviations) of the tensile strength and elongation at break of the NR composites decreased, whereas the hardness (Shore A) increased, for which extreme values were found in the sample with 100 phr Gd₂O₃ (3.34 ± 0.26 MPa, $411 \pm 9\%$, and 50 ± 1 , respectively). In order to determine the self-healing properties of the NR composites, the surfaces of the cut samples were gently pressed together, and they remained in contact for 60 min; then, the self-healing properties (the recoverable strength and the %Recovery) of the self-healed samples were measured, which were in the ranges of 0.30–0.40 MPa and 3.7–9.4%, respectively, for all the samples. These findings confirmed the ability to autonomously self-heal damaged surfaces through the generation of a reversible ionic supramolecular network. In summary, the outcomes from this work suggested that the developed Gd₂O₃/NR composites have great potential to be utilized as effective shielding materials, with additional dual shielding and self-healing capabilities that could prolong the lifetime of the materials, reduce the associated costs of repairing or replacing damaged equipment, and enhance the safety of all users and the public.

Keywords: natural rubber; Gd₂O₃; self-healing; shielding; mechanical properties; X-rays; neutrons



Citation: Poltabtim, W.; Thumwong, A.; Wimolmala, E.; Rattanapongs, C.; Tokonami, S.; Ishikawa, T.; Saenboonruang, K. Dual X-ray- and Neutron-Shielding Properties of Gd₂O₃/NR Composites with Autonomous Self-Healing Capabilities. *Polymers* **2022**, *14*, 4481. <https://doi.org/10.3390/polym14214481>

Academic Editor: Kamila Sałasińska

Received: 29 September 2022

Accepted: 19 October 2022

Published: 22 October 2022

Publisher's Note: MDPI stays neutral with regard to jurisdictional claims in published maps and institutional affiliations.



Copyright: © 2022 by the authors. Licensee MDPI, Basel, Switzerland. This article is an open access article distributed under the terms and conditions of the Creative Commons Attribution (CC BY) license (<https://creativecommons.org/licenses/by/4.0/>).

1. Introduction

As the demand for greener technologies has rapidly increased in recent years following the Sustainable Development Goals (SDGs) introduced by the United Nations

(UN) [1], radiation technologies have become one of the most sought-after tools to satisfy such demands due to their reduced use of hazardous chemicals during irradiation and procedures, adaptability to large-scale production, and vast range of applications, such as the determination of transfer mechanisms for minerals and radionuclides in plants [2,3], non-destructive imaging for cultural heritage artifacts [4], diagnostic and radiotherapy purposes for brain and breast cancers [5,6], measurement of moisture in soils [7], and gemstone modification [8]. However, despite their acknowledged benefits, excessive exposure to different types of radiation, especially those from neutrons and X-rays, can harmfully affect users and the public, possibly resulting in permanent injuries or deaths [9].

To minimize the risk of potential adverse effects from excessive radiation exposure, suitable and effective radiation-shielding equipment must be implemented in all nuclear-related facilities following a radiation safety concept, namely As Low As Reasonably Achievable, or ALARA [10]. Generally, the selection of the main materials and radiation-protective fillers used to produce radiation-shielding equipment depends on several factors, such as the type and energy of the incident radiation, as well as the physical and mechanical requirements for the intended applications. For example, to attenuate thermal neutrons (neutrons with an energy of 0.025 eV), compounds containing elements with a high neutron absorption cross-section (σ_{abs}), such as boron (B), boron carbide (B_4C), and boron oxide (B_2O_3), are often used due to the relatively high σ_{abs} value of B (^{10}B has a σ_{abs} value of 3840 barns, while $^{\text{nat}}\text{B}$ has a value of 768 barns) [11], which considerably enhances the absorption probabilities between incident thermal neutrons and the material. On the other hand, for X-ray attenuation, materials consisting of heavy elements or compounds, such as lead (Pb), lead oxide (PbO), bismuth oxide (Bi_2O_3), tungsten oxide (WO_3), and barium sulfate (BaSO_4), are commonly implemented due to the relatively high atomic numbers (Z) of Pb, Bi, W, and Ba ($Z = 82, 83, 74,$ and $56,$ respectively), as well as the high densities (ρ) of Pb, PbO, Bi_2O_3 , WO_3 , and BaSO_4 ($\rho = 11.3, 9.5, 8.9, 7.2,$ and 4.5 g/cm^3 , respectively) [12–14], which considerably enhance the interaction probabilities between incident X-rays and the material through two main mechanisms, namely photoelectric absorption and Compton scattering, subsequently resulting in improved X-ray-shielding properties of the composites [15].

While the use of these fillers can noticeably improve the radiation attenuation capabilities of materials, the lack of dual shielding properties (that is, the ability to effectively and simultaneously attenuate both thermal neutrons and X-rays) has resulted in the need to either acquire two distinct types of shielding materials or to mix two different fillers in the same material [16,17]. While these methods are possible, they could potentially increase the cost and space requirements to accommodate thicker materials, as well as possibly reducing desirable mechanical and physical properties of the shielding materials due to particle agglomeration from having filler contents that are too high [13]. To alleviate such drawbacks, gadolinium oxide (Gd_2O_3), which is a rare-earth compound, has drawn much attention from researchers and product developers in radiation safety due to the high values of σ_{abs} (49,700 barns) and Z (64) for Gd, as well as the high ρ of Gd_2O_3 (7.4 g/cm^3), which result in its ability to simultaneously attenuate both thermal neutrons and X-rays. Some examples of Gd_2O_3 used as radiation protective filler are the development of neutron-shielding hydrogels from poly(vinyl) alcohol (PVA), which indicated substantial enhancements in the ability of the hydrogels to attenuate thermal neutrons after the addition of Gd_2O_3 . This was evidenced by the half-value layer (HVL; the thickness of a material that can attenuate 50% of the initial intensity of radiation), which were reduced from 146.3 mm in a pristine PVA hydrogel to just 3.6 mm in a 10.5 wt% Gd_2O_3 /PVA hydrogel. Subsequently, this shielding improvement reduced space requirements to accommodate the materials by almost 40-fold [18]. Another work on the use of Gd_2O_3 by Kaewnuam et al. investigated the gamma-shielding properties of WO_3 - Gd_2O_3 - B_2O_3 glass and showed that the HVL values of the glasses were reduced from 1.424 cm in a sample with 17.5 wt% Gd_2O_3 to 1.326 cm in a sample with 27.5 wt% Gd_2O_3 determined based on 662 keV gamma rays emitted from ^{137}Cs [19]. These two examples clearly show the shielding effectiveness of Gd_2O_3 for

both thermal neutron and high-energy photon attenuations and present the advantages of Gd_2O_3 as a radiation-protective filler in comparison to common Pb, Bi, and B compounds.

Another important factor to consider in producing radiation-shielding materials is the selection of the main matrix, for which the selection largely depends on the requirements of the intended applications. For example, applications requiring high flexibility, strength, and elongation usually rely on natural rubber (NR) or synthetic rubber (SR). For example, B_2O_3 /NR [11], B_4C /NR [20], and H_3BO_3 /ethylene-propylene diene monomer (EPDM) [21] composites have been developed for use as flexible, neutron-shielding materials, while Bi_2O_3 /EPDM [13], WO_3 /EPDM [13], $BaSO_4$ /NR [14], and Pb /NR [22] composites have been utilized as flexible, X-ray-shielding and gamma-shielding materials. While these composites could serve their mandatory purpose (the ability to attenuate incident thermal neutrons or X-rays (depending on filler type) with high flexibility and strength), the lack of self-healing capabilities in most common NR and SR composites has resulted in extra procedures or new materials needed to restore full function once the materials are damaged, inevitably shortening their lifetimes and increasing operational costs. To resolve these shortcomings, Xu et al. successfully developed autonomously self-healing NR composites by introducing controlled peroxide-induced vulcanization to generate ionic cross-links to NR networks via the polymerization of zinc dimethacrylate (ZDMA), which slowed the formation of non-reversible covalent cross-links while generating a reversible ionic supramolecular network to NR, enabling the ability to autonomously heal after damage [23,24]. Hence, to expand their usefulness to other applications, the concept of autonomously self-healing NR materials can be adapted for the production of radiation-shielding materials, which could not only present the mentioned benefits but also improve safety for radiation users from damaged equipment.

Therefore, this current work investigates the properties of flexible Gd_2O_3 /NR composites for their potential use as dual thermal-neutron- and X-ray-shielding materials with autonomously self-healing capabilities by introducing reversible ionic supramolecular cross-links to NR networks. In order to understand the effects of the Gd_2O_3 fillers on the properties of the composites, the Gd_2O_3 contents were varied with values of 0, 25, 50, 75, and 100 parts per hundred parts of rubber (phr) by weight to thoroughly investigate the properties of interest, which consisted of thermal-neutron and X-ray-shielding properties (based on the linear attenuation coefficient (μ), the mass attenuation coefficient (μ_m), the half-value layer (HVL), the tenth-value layer (TVL), and the Pb equivalence (Pb_{eq})), as well as mechanical (based on tensile strength, elongation at break, and hardness (Shore A) both before and after self-healing), morphological, and physical (based on density) properties. The outcomes of this work can not only present valuable information on the dual neutron- and X-ray-shielding properties of the developed Gd_2O_3 /NR composites, but may also offer a novel procedure to obtain self-healing NR composites that is beneficial for the future development of other radiation-shielding products.

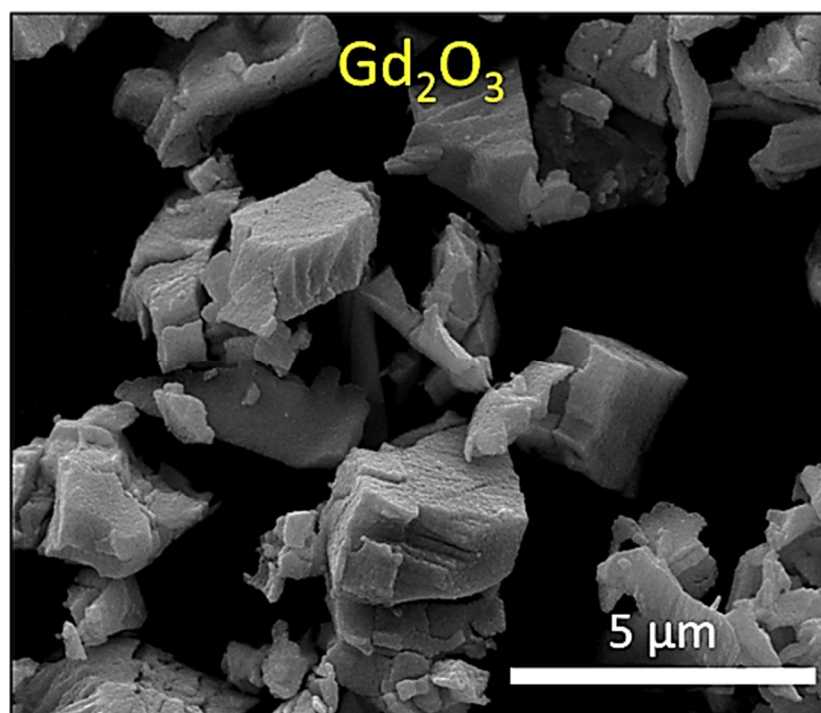
2. Experimental

2.1. Materials and Chemicals

Natural rubber (STR 5CV) with a Mooney viscosity of 60.8 (at 100 °C) was supplied by Hybrid Post Co., Ltd. (Bangkok, Thailand). The names, contents, roles, and suppliers of the chemicals used for sample preparation are shown in Table 1. An image of Gd_2O_3 powder captured using a scanning electron microscope (SEM; Quanta 450 FEI; JSM-6610LV, Eindhoven, the Netherlands) is shown in Figure 1, which indicates that the average particle size of the Gd_2O_3 powder was $3.4 \pm 0.4 \mu m$, as determined using ImageJ software version 1.50i (Bethesda, MD, USA).

Table 1. Material formulations of Gd₂O₃/NR composites and their chemical names, contents, roles, and suppliers.

Chemical	Content (phr)	Role	Supplier
Natural rubber (NR: STR 5CV)	100	Main matrix	Hybrid Post Co., Ltd. (Bangkok, Thailand)
Zinc dimethacrylate (ZDMA)	40	Accelerator	Shanghai Ruizheng Chemical Technology Co., Ltd. (Shanghai, China)
Dicumyl peroxide (DCP)	1	Curing agent	Shanghai Ruizheng Chemical Technology Co., Ltd. (Shanghai, China)
Gadolinium oxide (Gd ₂ O ₃)	0, 25, 50, 75, and 100	Radiation-protective filler	Shanghai Ruizheng Chemical Technology Co., Ltd. (Shanghai, China)

**Figure 1.** SEM image of Gd₂O₃ particles used in this work.

2.2. Sample Preparation

The NR samples were prepared using two steps: mastication and then compounding. Initially, the NR was masticated on a two-roll mill (R11-3FF, Kodaira Seisakusho Co., Ltd., Tokyo, Japan) for 5 min. Then, the masticated NR was compounded with the chemicals (Table 1) for a further 15–20 min. Notably, although the content of Gd₂O₃ was as high as 100 phr, the much higher density of Gd₂O₃ ($\rho = 7.4 \text{ g/cm}^3$) than that of NR (approximately $0.93\text{--}0.97 \text{ g/cm}^3$ [25]) resulted in the volume of Gd₂O₃ powder used during the compounding being much less than that of NR, making the mixing of all the chemicals on a two-roll mill possible. After the compounding, the NR samples were vulcanized using hot compression molding (CC-HM-2060, Chaicharoen Karnchang Co., Ltd., Bangkok, Thailand) at 150 °C and a pressure of 160 kg/cm² for 150 secs in a mold with dimensions of either 15 cm × 15 cm × 0.2 cm or 10 cm × 10 cm × 0.2 cm. Notably, the procedure for sample preparation was mainly based on the published works of Xu et al. [23,24], while the cure time of 150 secs was selected following preliminary studies for optimized cure times, for which shorter or longer cure times resulted in the samples being too soft or too hard, respectively, which limited their useability and prevented the initiation of self-healing mechanisms from occurring [26].

2.3. Characterization

2.3.1. Neutron-Shielding Properties

The neutron shielding properties of the Gd_2O_3/NR composites were investigated at the Thailand Institute of Nuclear Technology (Public Organization), Bangkok, Thailand. The neutron-shielding parameters investigated in this work were the neutron transmission (I/I_0), the linear attenuation coefficient (μ), the half-value layer (HVL), and the tenth-value layer (TVL), and their relationships are shown in Equations (1)–(4) [14]:

$$I/I_0 = e^{-\mu x} \quad (1)$$

$$HVL = \frac{\ln(2)}{\mu} \quad (2)$$

$$\mu_m = \frac{\mu}{\rho} \quad (3)$$

$$TVL = \frac{\ln(10)}{\mu} \quad (4)$$

where I_0 is the initial intensity of the incident neutrons, I is the final intensity of the transmitted neutrons, x is the thickness of the sample, and ρ is the density of the sample.

The setup for neutron-shielding measurement is schematically shown in Figure 2, with a $^{241}Am/Be$ used as a thermal neutron source. The values of I and I_0 were recorded using a 3He neutron detector that was connected to a high-voltage supplier (Model 659, ORTEC, CA, USA), an amplifier (Model 2022, Canberra, CT, USA), and a time counter (Model TC 535P, Tennelec, TN, USA). The neutron source was positioned such that it was 0.89 m away from the NR sample and 1.00 m away from the detector. Notably, to investigate the effects of sample thickness on the neutron-shielding properties, the total thickness values of the NR samples were also varied (2, 4, 6, 8, and 10 mm).

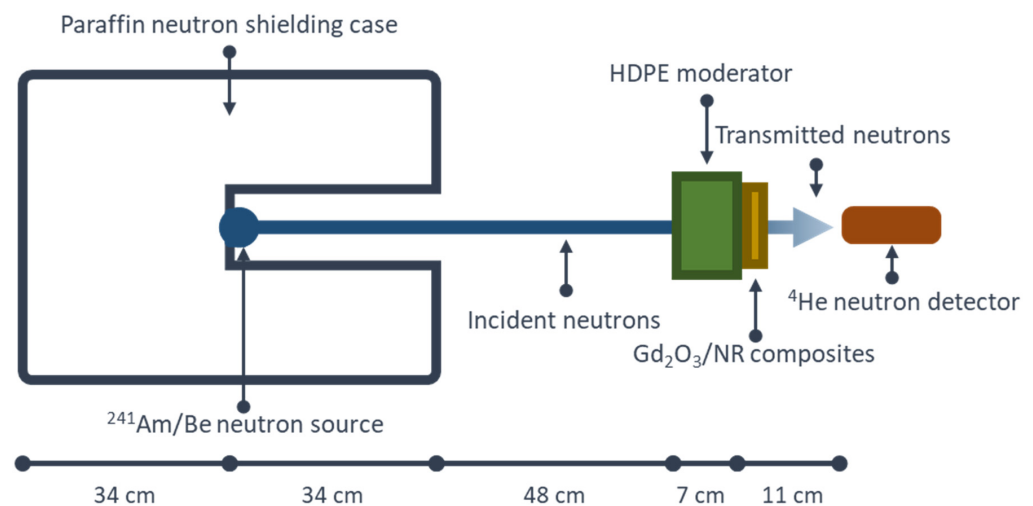


Figure 2. Schematic setup for neutron-shielding measurement.

2.3.2. X-ray-Shielding Properties

The schematic setup for X-ray-shielding measurement is shown in Figure 3. The measurement was carried out at the Secondary Standard Dosimetry Laboratory (SSDL), the Office of Atoms for Peace (OAP), Bangkok, Thailand. The X-ray-shielding parameters investigated in this work were X-ray transmission (I/I_0), the linear attenuation coefficient (μ), the mass attenuation coefficient (μ_m), the half-value layer (HVL), the tenth-value layer (TVL), and the Pb equivalence (Pb_{eq}), for which Pb_{eq} could be determined using Equation (5) [14]:

$$Pb_{eq} = \frac{\mu x}{\mu_{Pb}} \quad (5)$$

where μ_{Pb} is the linear attenuation coefficient of a pure Pb sheet. It should be noted that the values of μ_{Pb} were 63.06 cm^{-1} and 25.99 cm^{-1} for the incident X-ray energies of 45 keV and 80 keV, respectively, and were numerically determined using XCOM software (National Institute of Standards and Technology, Gaithersburg, MD, USA) [14,27]. The X-ray energies of 45 keV and 80 keV were selected for the determination of Pb_{eq} due to being the average energies of X-rays generated from an X-ray tube (YXLON MGC41, NY, USA) with the supplied voltages of 60 and 100 kV (Keithley 651B, OH, USA), respectively, used in this work. The emitted X-ray beam was collimated using a Pb collimator with a 1 mm pinhole, and the transmitted X-rays were detected and counted using a free-air ionization chamber (Korea Research Institute of Standards and Science; KRISS, Daejeon, Korea). More details for the setup of the neutron-shielding measurement are available in [14]. Similar to the neutron measurement, the total thickness values of the NR samples varied from 2 to 10 mm in 2 mm increments to investigate effects of material thickness on X-ray-shielding abilities.

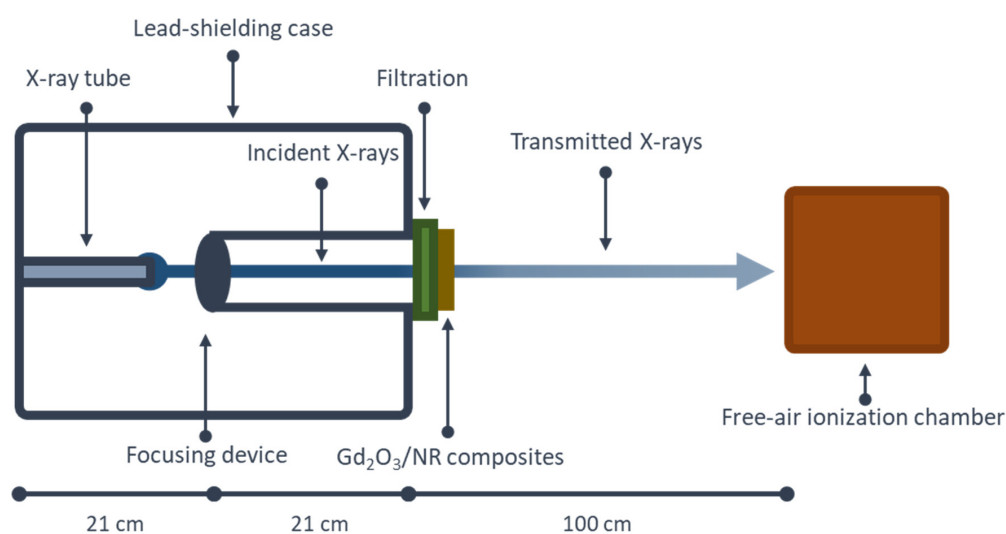


Figure 3. Schematic setup for X-ray-shielding measurement.

2.3.3. Mechanical Properties

The mechanical properties of tensile strength and elongation at break for all the Gd₂O₃/NR composites were determined using a universal testing machine (Auto-graph AG-I 5kN, Shimadzu, Kyoto, Japan) following ASTM D412-06 standard testing. The tensile testing speed used for all the samples was 50 mm/min. The surface hardness (Shore A) was determined using a hardness durometer (Teclock GS-719G, Japan) following the ASTM D2240-05 standard testing method.

For the determination of the self-healing capabilities of the developed Gd₂O₃/NR composites, samples having shapes and sizes based on ASTM D412-06 standard testing were cut into two equal pieces using a surgical knife and were immediately brought into contact. Then, after 60 min of contact, the samples were installed in a universal testing machine (Auto-graph AG-I 5kN, Shimadzu, Kyoto, Japan) to determine their tensile strength and elongation at break, following the same testing procedures as those for the uncut samples. Then, the tensile strength values of the self-healed samples were used for the calculation of the percentage of recoverable strength (%Recovery) using Equation (6) [18]:

$$\% \text{Recovery} = \frac{\text{TS}_{\text{self-healing}}}{\text{TS}_{\text{uncut}}} \times 100\% \quad (6)$$

where $\text{TS}_{\text{self-healing}}$ and TS_{uncut} are the tensile strengths of the self-healed and uncut samples, respectively [28].

2.3.4. Density Measurement

The densities for all the Gd₂O₃/NR composites were determined using a densitometer (MH-300A, Shanghai, China) with a precision of 0.01 g/cm³, and the determination was carried out based on the Archimedes principle [29]. Additionally, to verify the correctness of the density measurement, theoretical densities (ρ_{th}) for all the samples were calculated using Equation (7) [14]:

$$\rho_{th} = \frac{C_{NR} + C_{Gd2O3}}{\frac{C_{NR}}{\rho_{NR}} + \frac{C_{Gd2O3}}{\rho_{Gd2O3}}} \tag{7}$$

where C_{NR} is the content of NR, C_{Gd2O3} is the content of Gd₂O₃, ρ_{NR} is the density of NR (0.95 g/cm³), and ρ_{Gd2O3} is the density of Gd₂O₃ (7.4 g/cm³).

2.3.5. Morphological Studies

The morphology, dispersion of Gd₂O₃ particles, and dispersion of Gd elements were determined using scanning electron microscopy (SEM) with energy-dispersive X-ray (EDX) spectroscopy (Quanta 450 FEI: JSM-6610LV, Eindhoven, the Netherlands) at a 10 kV accelerating voltage. Prior to the SEM-EDX studies, all specimens were coated with gold using a sputter coater (Quorum SC7620: Mini Sputter Coater/Glow Discharge System, Nottingham, UK) at a power voltage of 10 kV and a current of 10 mA for 120 secs.

3. Results and Discussion

3.1. Density

Table 2 indicates the experimental and theoretical densities, as well as the differences between these two values, of all the Gd₂O₃/NR composites investigated in this work. The results showed that the densities of the NR samples increased with increasing Gd₂O₃ content, while the differences between the experimental and theoretical values were below 5.0% for all the samples, clearly verifying the correctness and reliability of the experimental values for further use. The positive relationship between density and filler content was due to the much higher density of Gd₂O₃ than NR, resulting in a greater sample mass (determined at the same total volume) and, subsequently, greater overall density of the NR composites containing higher Gd₂O₃ contents [30].

Table 2. Experimental and theoretical densities, as well as the differences between the methods, of Gd₂O₃/NR composites with varying Gd₂O₃ contents of 0, 25, 50, 75, and 100 phr. Experimental densities shown as mean ± standard deviation.

Gd ₂ O ₃ Content (phr)	Experimental Density (g/cm ³)	Theoretical Density (g/cm ³)	Difference (%)
0 (Control)	0.99 ± 0.01	0.95	4.0
25	1.19 ± 0.01	1.15	3.4
50	1.35 ± 0.01	1.33	1.5
75	1.49 ± 0.01	1.51	1.3
100	1.60 ± 0.01	1.68	5.0

3.2. Neutron-Shielding Properties

The results for the neutron-shielding properties, consisting of I/I₀, μ , μ_m , HVL, and TVL, for all the Gd₂O₃/NR composites are shown in Figure 4, which indicates that the overall neutron-shielding properties of the samples increased with increasing Gd₂O₃ content, as evidenced by the lower values of I/I₀, HVL, and TVL and the higher values of μ and μ_m in the samples containing higher contents of Gd₂O₃. This shielding enhancement from the addition of Gd₂O₃ was mainly due to Gd having a much higher σ_{abs} value than the C and H in NR (σ_{abs} values for Gd, C, and H are 49,700 barns, 0.0035 barns, and 0.3326 barns, respectively [31]), resulting in considerably increased chances for incident thermal neutrons to be absorbed and attenuated by the composites and, consequently, leading to superior neutron-shielding properties for the Gd₂O₃/NR composites [32]. Figure 5 shows the disper-

sion of Gd in the NR composites based on SEM-EDX and reveals that the highest elemental density of Gd was in the sample containing 100 phr Gd_2O_3 (Figure 5d), confirming the rationale for the improved neutron-shielding properties of the Gd_2O_3 /NR composites by the addition of Gd_2O_3 .

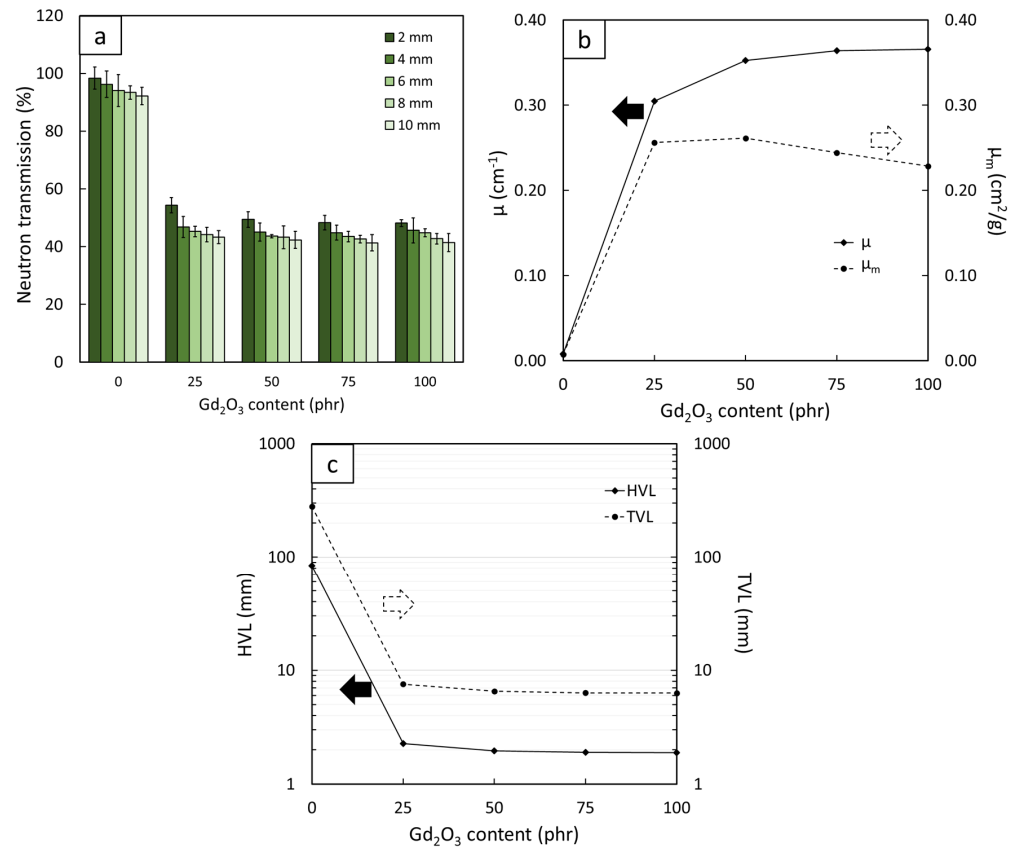


Figure 4. Neutron-shielding properties: (a) the neutron transmission, (b) linear attenuation coefficient (μ), mass attenuation coefficient (μ_m), (c) half-value layer (HVL) and tenth-value layer (TVL) of Gd_2O_3 /NR composites containing varying Gd_2O_3 contents of 0, 25, 50, 75, and 100 phr, where error bars indicate \pm standard error.

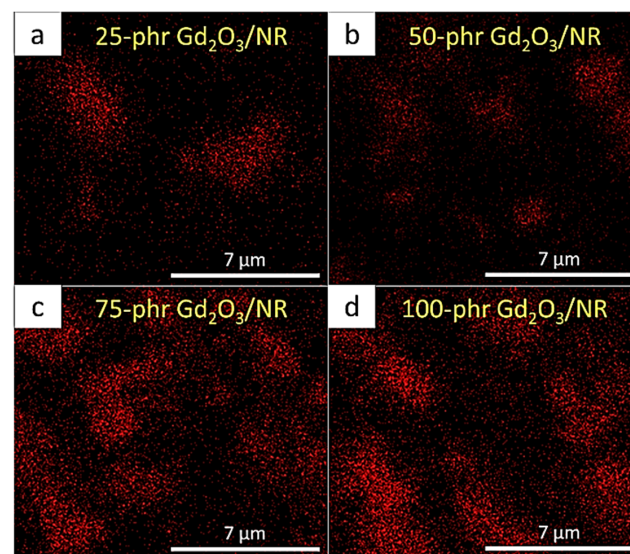


Figure 5. Dispersion of Gd_2O_3 /NR composites containing varying Gd_2O_3 contents captured using SEM-EDX: (a) 25 phr, (b) 50 phr, (c) 75 phr, and (d) 100 phr.

In addition, Figure 4 indicates that a small addition of 25 phr Gd_2O_3 to pristine NR could sharply increase the neutron-shielding properties of the samples, as seen by the sharp decreases in I/I_0 and HVL from 97% and 84 mm in pristine NR to just 55% and 2.3 mm, respectively, in the 25 phr $\text{Gd}_2\text{O}_3/\text{NR}$ sample (values of I/I_0 and HVL were compared using 2 mm thick samples). This notable improvement in the neutron-shielding properties was mainly due to the sudden change in dominant neutron interactions from elastic scattering in the pristine NR to neutron absorption in the $\text{Gd}_2\text{O}_3/\text{NR}$ composites, for which the latter mechanism was relatively more effective in neutron attenuation than the former [33]. However, as more Gd_2O_3 powder was added to the composites, only a slight improvement was observed, perhaps because the samples already relied on the preferable absorption mechanism such that further addition of Gd_2O_3 could only slightly increase the probabilities of neutrons being absorbed [34].

Another point worth mentioning is that the ability to attenuate neutrons increased with increasing sample thickness. The dependence of neutron-shielding properties on sample thickness, as illustrated in the determination of I/I_0 and shown in Figure 4a, was mostly due to more materials being available to elastically scatter (in the case of a pristine NR sample) or absorb (in the case of $\text{Gd}_2\text{O}_3/\text{NR}$ samples) incident neutrons in thicker samples, subsequently reducing the transmitted neutrons (lower I/I_0). This relationship could also be mathematically explained using Equation (1) when re-arranged as shown in Equation (8), which depicts that the value of $\ln(I/I_0)$ was inversely proportional to x (thickness of the sample); hence, I/I_0 was negatively related to x :

$$\ln(I/I_0) = -\mu x \quad (8)$$

3.3. X-ray-Shielding Properties

Figure 6 shows the results for the percentage of X-ray transmission for 60 kV and 100 kV X-rays, respectively, through varying thicknesses (2, 4, 6, 8, and 10 mm) of $\text{Gd}_2\text{O}_3/\text{NR}$ composites. Similar to the results from the neutron-shielding measurement, the X-ray transmission decreased with increasing Gd_2O_3 content and sample thickness. The dependence of the X-ray transmission on Gd_2O_3 content was mainly due to the increased interaction probabilities between the incident X-rays and the materials through photoelectric absorption and Compton scattering with the addition of Gd_2O_3 , for which their cross-sections were positively correlated to the Z and ρ values of the materials, hence improving the attenuation ability of the composites [35,36]. In addition, increasing the thickness of the samples could decrease X-ray transmission due to more Gd_2O_3 being available to interact with the incident X-rays, resulting in fewer X-rays being transmitted through the samples.

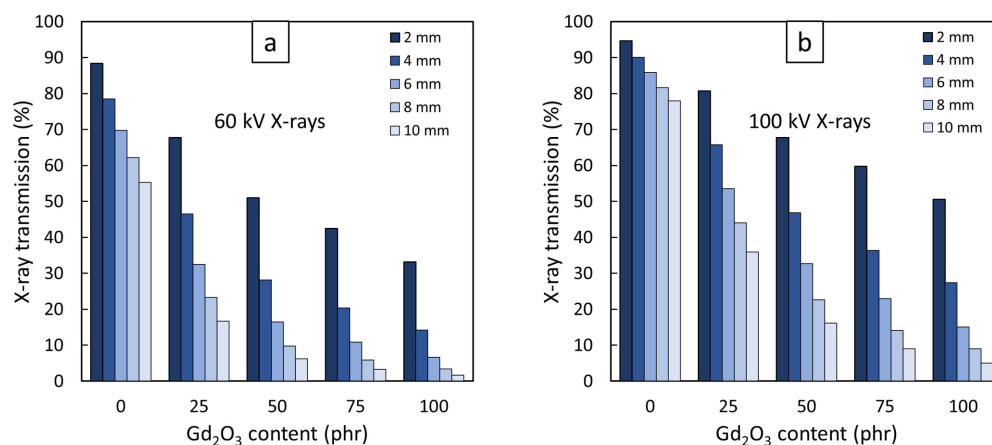


Figure 6. X-ray transmission of $\text{Gd}_2\text{O}_3/\text{NR}$ composites with varying thicknesses from 2 to 10 mm and varying Gd_2O_3 contents from 0 to 100 phr determined at X-ray supplied voltages of (a) 60 kV and (b) 100 kV.

Figure 7 shows the results of the μ , μ_m , HVL, TVL, and Pb_{eq} values of Gd_2O_3/NR composites containing varying Gd_2O_3 content determined using 60 kV and 100 kV X-rays (common supplied voltages used for medical diagnostics [37]). The results imply that the overall X-ray-shielding properties of the composites generally increased with increasing Gd_2O_3 content, as evidenced by the lowest values of HVL and TVL and the highest values of μ , μ_m , and Pb_{eq} being found in the sample with 100 phr Gd_2O_3 . For example, the values of HVL (Pb_{eq}) of the NR composites were reduced from 1.12 cm and 2.50 cm, respectively, (0.03 mmPb and 0.03 mmPb) for pristine NR to 0.36 and 0.65 cm (0.09 mmPb and 0.12 mmPb) for 25 phr Gd_2O_3/NR composites, determined at 60 kV and 100 kV X-rays, respectively, exhibiting approximately a 3–4-fold improvement in X-ray attenuation ability with the addition of just 25 phr Gd_2O_3 .

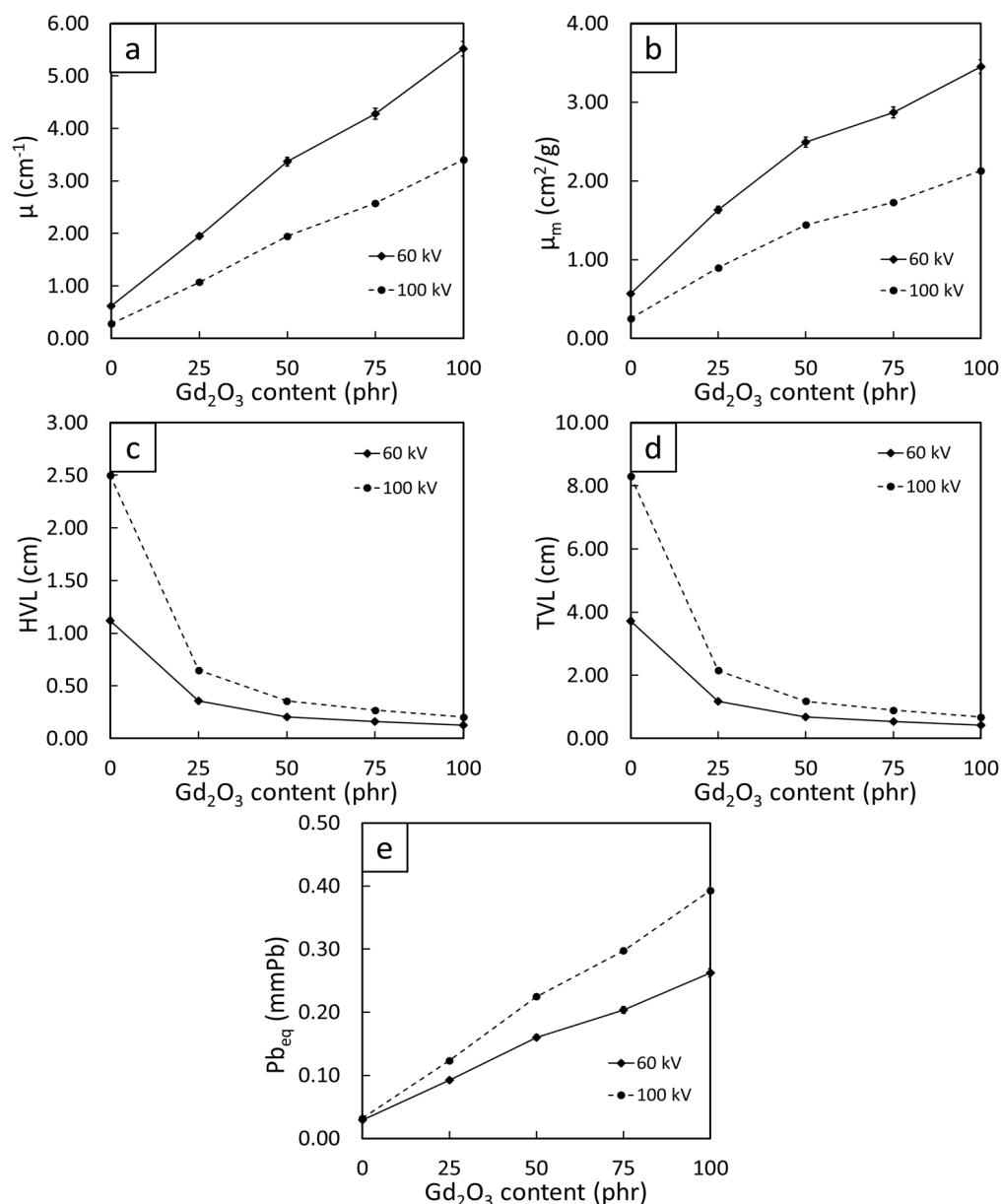


Figure 7. X-ray-shielding properties: (a) linear attenuation coefficient (μ), (b) mass attenuation coefficient (μ_m), (c) half-value layer (HVL), (d) tenth-value layer (TVL), and (e) lead equivalence (Pb_{eq}) of 3 mm thick Gd_2O_3/NR composites containing varying Gd_2O_3 contents of 0, 25, 50, 75, and 100 phr.

Another interesting result from Figure 7 was that the X-ray-shielding properties of the samples determined at the 60 kV supplied voltage were higher than those at the 100 kV supplied voltage due to the cross-section of the dominant photoelectric absorption (σ_{pe}) being inversely related to the cube of incident X-ray energy (E), as shown in Equation (9) [38]:

$$\sigma_{pe} \propto \frac{Z^n}{E^3} \quad (9)$$

Consequently, the incident X-rays emitted from an X-ray tube with higher supplied voltages could have fewer chances of interaction with the materials, resulting in more X-rays being transmitted and, subsequently, lower overall X-ray attenuation properties than lower-energy X-rays [39]. Notably, the values of Pb_{eq} at a specific Gd_2O_3 content could be tailored according to the shielding requirements for intended applications by lowering or increasing the thickness of the sample (the sample thickness for Figure 7e was 3 mm) using Equation (5).

3.4. Comparative Neutron- and X-ray-Shielding Properties between Current and Other Similar Materials

Table 3 shows a comparison of neutron- and X-ray-shielding properties (based on the values of HVL) from this work with other similar materials, which indicates that the current materials exhibited comparable or better neutron and X-ray attenuation capabilities than those from other reports. As a result, this comparison clearly confirmed the useability and potential of the NR composites for utilization as effective neutron- and X-ray-shielding materials with potential self-healing capabilities. It should be noted that the differences in the HVL values from all the materials in Table 3 could be due to several factors, such as differences in the filler types and contents used, as well as various energies of the incident radiation during measurement.

Table 3. Comparison of neutron- and X-ray-shielding properties based on the half-value layer (HVL) between the results from this work and those from similar materials. Numbers in parentheses represent supplied voltages used for X-ray-shielding measurement.

Main Matrix	Filler	Filler Content	Half-Value Layer (mm)		Reference
			Neutrons	X-rays	
NR	Gd_2O_3	50 phr	2.0	2.1 (60 kV)/ 3.6 (100 kV)	This work
NR	Gd_2O_3	75 phr	1.9	1.6 (60 kV)/ 2.7 (100 kV)	This work
NR	B_2O_3	80 phr	3.2	–	[11]
PVA	Sm_2O_3	10.5 wt%	4.2	–	[18]
PVA	Gd_2O_3	10.5 wt%	3.6	–	[18]
EPDM	B_2O_3	42.6 phr	3.7	–	[40]
NR	Bi_2O_3	50 phr	–	6.0 (60 kV)	[14]
NR	$BaSO_4$	50 phr	–	6.0 (60 kV)	[14]
NR	Bi_2O_3	40 phr	–	~3.5 (120 kV)	[41]
NR	Bi_2O_3	80 phr	–	~3.0 (120 kV)	[41]

3.5. Mechanical Properties

Table 4 shows the mechanical properties—tensile strength, elongation at break, and hardness (Shore A) of Gd_2O_3 /NR composites containing varying Gd_2O_3 contents (0, 25, 50, 75, and 100 phr). The results indicate that the values of tensile strength and elongation at break generally decreased, while the hardness (Shore A) increased with increasing Gd_2O_3 content. The decreases in tensile properties after the addition of Gd_2O_3 could be due to poor surface compatibility between Gd_2O_3 and the NR matrix, which possibly resulted in the formation of voids and discontinuities in the matrix, subsequently obstructing the transfer of external forces and reducing the overall strength and elongation of the materials [42]. Furthermore, the addition of high levels of Gd_2O_3 contents, especially at 100 phr, led to high

agglomeration of the Gd_2O_3 particles due to filler–filler interactions that prevented more preferable and stronger rubber–filler interactions from occurring [43]. The SEM images depicting the dispersion of Gd_2O_3 particles in the NR matrix are shown in Figure 8 and reveal that, while the particles were fairly evenly distributed throughout the NR matrix, some particle agglomeration was found in samples with higher filler contents, especially at 50, 75, and 100 phr (Figure 8c–e), compared to pristine NR (Figure 8a) and the sample with 25 phr filler content (Figure 8b). On the other hand, hardness (Shore A) had a strong positive relationship with Gd_2O_3 content due to the high rigidity of the Gd_2O_3 particles, which enhanced the overall rigidity and, hence, the hardness of the composites [44]. These findings are consistent with other reports, where the mechanical properties of materials generally decrease with the addition of high filler content, especially those developed for use in radiation protection [13,14].

Table 4. Mechanical properties of tensile strength, elongation at break, and hardness (Shore A) of Gd_2O_3 /NR composites containing varying Gd_2O_3 contents of 0, 25, 50, 75, and 100 phr. Values are shown as mean \pm standard deviation.

Gd_2O_3 Content (phr)	Tensile Strength (MPa)	Elongation at Break (%)	Hardness (Shore A)
0 (Control)	8.29 \pm 0.83	555 \pm 53	38 \pm 1
25	5.02 \pm 0.79	387 \pm 33	41 \pm 1
50	4.07 \pm 0.14	515 \pm 10	45 \pm 1
75	4.08 \pm 0.77	463 \pm 16	46 \pm 1
100	3.34 \pm 0.26	411 \pm 9	50 \pm 1

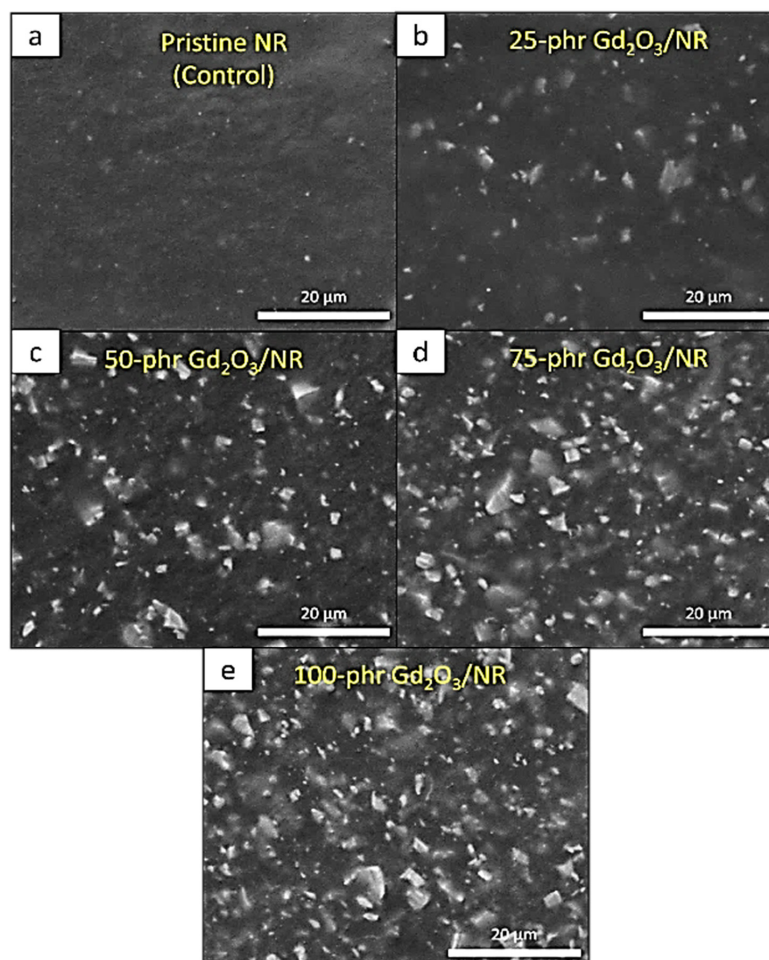


Figure 8. SEM images showing morphology and particle dispersion of NR composites containing varying Gd_2O_3 contents: (a) 0, (b) 25 phr, (c) 50 phr, (d) 75 phr, and (e) 100 phr.

Comparing the tensile properties obtained from this work with another work by Xu et al. indicated that the current pristine NR samples were approximately four times higher in tensile strength, as evidenced by the values reported in [23,24] being lower than 2 MPa for all the formulations. The differences in mechanical properties between these two works could be due to several factors, such as different formulation and cure times, as well as the types of NR used for sample preparation, which can affect the degree of cross-linking and, hence, the strength of the composites [45].

3.6. Self-Healing Properties

Figure 9 shows the comparative values of strength and elongation at break, as well as the percentage of recoverable strength (%Recovery), of the original and 60 min self-healed NR composites containing varying Gd_2O_3 contents (0, 25, 50, 75, and 100 phr). The results indicate that the values of tensile strength and elongation at break for all the self-healed samples (Figure 9a,b) were lower than the original ones, with values for recoverable strength and elongation at break in the ranges of 0.30–0.40 MPa and 22.6–36.4%, respectively, leading to values of %Recovery in the range of 3.7–9.4% (Figure 9c).

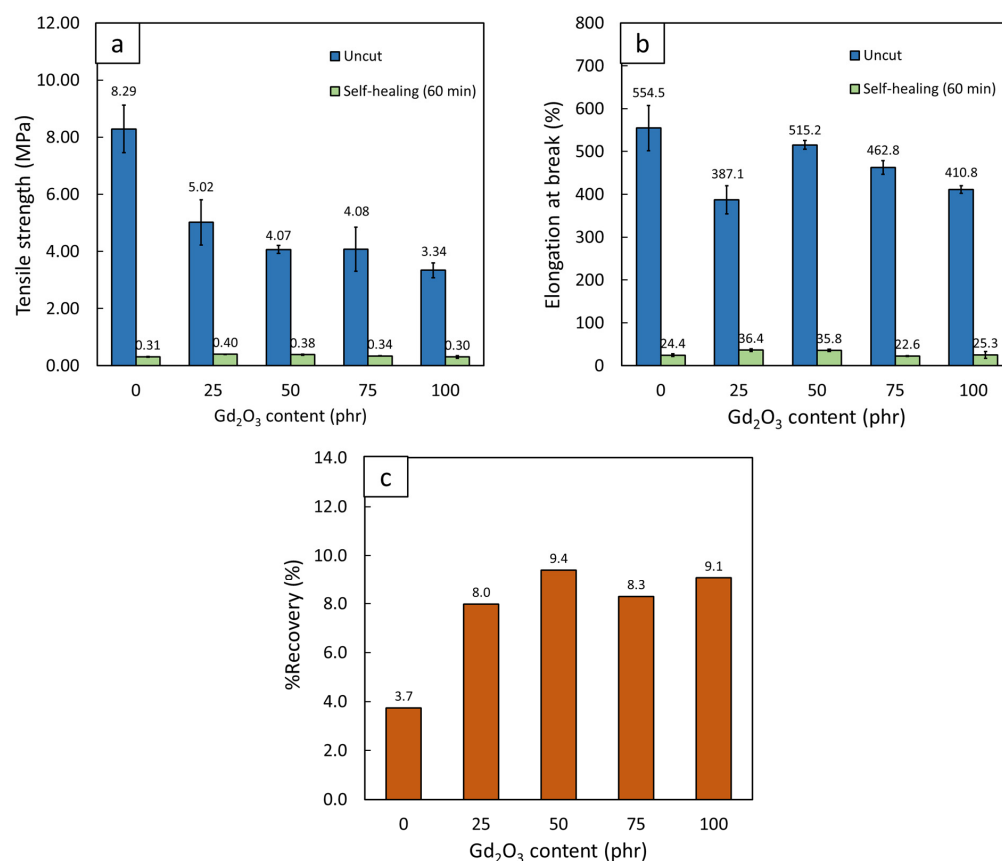


Figure 9. Comparison of (a) tensile strength, (b) elongation at break, and (c) percentage of recovery (%Recovery) for uncut and self-healed Gd_2O_3 /NR composites containing varying Gd_2O_3 contents (0, 25, 50, 75, and 100 phr), where error bars indicate \pm standard deviation.

The reduction in the tensile strength and elongation at break of the self-healed NR composites in comparison to the original samples could be explained by the NR molecular chains in the uncut samples being originally cross-linked with a combination of covalent and ionic bonds, which resulted in relatively high tensile strength and elongation at break before the cut [46]. However, as the two damaged surfaces were gently pressed together and remained in contact for 60 min at room temperature (approximately 25 °C), a reversible ionic supramolecular network via the polymerization of ZDMA was able to recreate the sample through the mobility of NR molecular chains and, subsequently, restore some

recoverable strength to the self-healed surfaces [47]. Nonetheless, the overall strengths of the self-healed samples were considerably lower than the original samples, with %Recovery values in the range of 3.7–9.1% (Figure 9c). This could be due to the reduced level of cross-link density in the samples after self-healing that could only be recreated by ionic bonds. On the other hand, the covalent bonds, which also initially presented and played major roles in providing exceptional strength to the original samples, were irreversible and, consequently, absent in the self-healed contact, resulting in much-reduced levels of recoverable strength and elongation at break for the samples [48]. Another factor that affected the self-healing mechanism was the addition of the Gd₂O₃ particles to the NR matrix, for which the fillers were not a part of the reversible supramolecular network and, hence, hindered or blocked the initiation of self-healing [24].

Nonetheless, despite having Gd₂O₃ contents of up to 100 phr, the recoverable strengths of the Gd₂O₃/NR composites were in the range of 0.30–0.40 MPa, which were in the same order of magnitude as that of pristine NR reported by Xu et al. (being in the range of 0.5–0.7 MPa, depending on self-healing times [23]), implying the useability and potential of the current self-healing materials for applications in radiation protection. Furthermore, the success of the current work could promote further attempts to develop ‘smart’ and more effective materials for use in radiation shielding, along with the previously reported composites of Bi₂O₃/PVA, Sm₂O₃/PVA, Gd₂O₃/PVA, graphene/PVA, and PbO₂/acrylamide [18,28,49,50]. It should be noted that the %Recovery values of the NR samples with the addition of Gd₂O₃ were higher than that of the pristine NR because the original Gd₂O₃/NR composite had 2–3 times lower tensile strength than pristine NR, while having similar recoverable strength after self-healing, which resulted in considerably higher %Recovery values for the Gd₂O₃/NR composites.

4. Conclusions

This work developed dual neutron-shielding and X-ray-shielding NR composites containing varying contents of Gd₂O₃ (0, 25, 50, 75, and 100 phr) with autonomously self-healing capabilities. The results showed that the added Gd₂O₃ acted as an effective protective filler against neutrons and X-rays, as evidenced by the decreases in I/I₀, HVL, and TVL and the increases in μ , μ_m , and Pb_{eq} of the NR composites after being added to the matrix. In addition, the results indicated that the increased filler content led to decreased tensile strength and elongation at break, whereas the hardness (Shore A) increased, mainly due to the initiation of particle agglomeration at high filler contents and poor surface compatibility between the NR matrix and the filler. The developed NR composites also offered self-healing capabilities at the fractured surfaces through a reversible ionic supramolecular network, with recoverable strength and %Recovery values in the ranges 0.30–0.4 MPa and 3.7–9.4%, respectively (after self-healing for 60 min). Based on the overall results obtained, the developed Gd₂O₃/NR composites showed great potential for use as novel and self-healing radiation-shielding materials that could effectively attenuate both neutrons and X-rays, thus prolonging the lifetime of the protective material and enhancing the safety for users, as well as being a basis for the future development of ‘smart’ shielding materials.

Author Contributions: Conceptualization, K.S.; formal analysis, W.P., A.T., E.W., C.R., S.T., T.I. and K.S.; funding acquisition, K.S.; investigation, W.P., A.T., E.W., C.R., S.T., T.I. and K.S.; methodology, W.P., A.T., E.W., C.R., S.T., T.I. and K.S.; supervision, K.S.; validation, W.P., A.T., E.W., C.R., S.T., T.I. and K.S.; visualization, K.S.; writing—original draft, K.S.; writing—review and editing, W.P., A.T., E.W., C.R., S.T., T.I. and K.S. All authors have read and agreed to the published version of the manuscript.

Funding: This research was financially supported by the Office of the Ministry of Higher Education, Science, Research, and Innovation; the Thailand Science Research and Innovation through the Kasetsart University Reinventing University Program 2021; and the Kasetsart University Research and Development Institute (KURDI), Bangkok, Thailand (grant number FF(KU)25.64).

Institutional Review Board Statement: Not applicable.

Informed Consent Statement: Not applicable.

Data Availability Statement: The data presented in this study are available on request from the corresponding author.

Acknowledgments: The Kasetsart University Research and Development Institute (KURDI) and the Specialized Center of Rubber and Polymer Materials in Agriculture and Industry (RPM) provided publication support.

Conflicts of Interest: The authors declare no conflict of interest.

References

1. Pradhan, P.; Costa, L.; Rybski, D.; Lucht, W.; Kropp, J.P. A systematic study of sustainable development goal (SDG) interactions. *Earth's Future* **2017**, *5*, 1169–1179. [[CrossRef](#)]
2. Courbet, G.; Gallardo, K.; Vigani, G.; Brunel-Muguet, S.; Trouverie, J.; Salon, C.; Ourry, A. Disentangling the complexity and diversity of crosstalk between sulfur and other mineral nutrients in cultivated plants. *J. Exp. Bot.* **2019**, *70*, 4183–4196. [[CrossRef](#)] [[PubMed](#)]
3. Saenboonruang, K.; Phonchanthuek, E.; Prasandee, K. Soil-to-plant transfer factors of natural radionuclides (^{226}Ra and ^{40}K) in selected Thai medicinal plants. *J. Environ. Radioact.* **2018**, *184–185*, 1–5. [[CrossRef](#)] [[PubMed](#)]
4. Jassens, K.; Dik, J.; Cottee, M.; Susini, J. Photon-based techniques for nondestructive subsurface analysis of painted cultural heritage artifacts. *Acc. Chem. Res.* **2010**, *43*, 814–825. [[CrossRef](#)]
5. Kut, C.; Chaichana, K.; Xi, J.; Raza, S.M.; Ye, X.; McVeigh, E.R.; Rodriguez, F.J.; Quinones-Hinojosa, A.; Li, X. Detection of human brain cancer infiltration ex vivo and in vivo using quantitative optical coherence tomography. *Sci. Transl. Med.* **2015**, *7*, 292ra100. [[CrossRef](#)]
6. Taylor, C.W.; Kirby, A.M. Cardiac side-effects from breast cancer radiotherapy. *Clin. Oncol.* **2015**, *27*, 621–629. [[CrossRef](#)]
7. Lekshmi, S.; Singh, D.N.; Baghini, M.S. A critical review of soil moisture measurement. *Measurement* **2014**, *54*, 92–105.
8. Parejo Calvo, W.A.; Duarte, C.L.; Machado, L.D.B.; Manzoli, J.E.; Geraldo, A.B.C.; Kodama, Y.; Silva, L.G.A.; Pino, E.S.; Somessari, E.S.R.; Silveira, C.G.; et al. Electron beam accelerators—trends in radiation processing technology for industrial and environmental applications in Latin America and the Caribbean. *Radiat. Phys. Chem.* **2012**, *81*, 1276–1281. [[CrossRef](#)]
9. Leuraud, K.; Richardson, D.B.; Cardis, E.; Daniels, R.D.; Gillies, M.; O'Hagan, J.A.; Hamra, G.B.; Haylock, R.; Laurier, D.; Moissonnier, M.; et al. Ionising radiation and risk of death from leukaemia and lymphoma in radiation-monitored workers (INWORKS): An international cohort study. *Lancet Haematol.* **2015**, *2*, e276–e281. [[CrossRef](#)]
10. Yeung, A.W.K. The “As Low As Reasonably Achievable” (ALARA) principle: A brief historical overview and a bibliometric analysis of the most cited publications. *Radioprotection* **2019**, *54*, 103–109. [[CrossRef](#)]
11. Ninyong, K.; Wimolmala, E.; Sombatsompop, N.; Saenboonruang, K. Potential use of NR and wood/NR composites as thermal neutron shielding materials. *Polym. Test.* **2017**, *59*, 336–343. [[CrossRef](#)]
12. Kumar, A. Gamma ray shielding properties of $\text{PbO-Li}_2\text{O-B}_2\text{O}_3$ glasses. *Radiat. Phys. Chem.* **2017**, *136*, 50–53. [[CrossRef](#)]
13. Poltabtim, W.; Wimolmala, E.; Saenboonruang, K. Properties of lead-free gamma-ray shielding materials from metal oxide/EPDM rubber composites. *Radiat. Phys. Chem.* **2018**, *153*, 1–9. [[CrossRef](#)]
14. Thumwong, A.; Chinnawet, M.; Intarasena, P.; Rattanapongs, C.; Tokonami, S.; Ishikawa, T.; Saenboonruang, K. A comparative study on X-ray shielding and mechanical properties of natural rubber latex nanocomposites containing Bi_2O_3 or BaSO_4 : Experimental and numerical determination. *Polymers* **2022**, *14*, 3654. [[CrossRef](#)]
15. Singh, V.P.; Ali, A.M.; Badiger, N.M.; Al-Khayatt, A.M. Monte Carlo simulation of gamma ray shielding parameters of concretes. *Nucl. Eng. Des.* **2013**, *265*, 1071–1077. [[CrossRef](#)]
16. Hu, G.; Shi, G.; Hu, H.; Yang, Q.; Yu, B.; Sun, W. Development of gradient composite shielding material for shielding neutrons and gamma rays. *Nucl. Eng. Technol.* **2020**, *52*, 2387–2393. [[CrossRef](#)]
17. Tekin, H.O.; Altunsoy, E.E.; Kavaz, E.; Sayyed, M.I.; Agar, O.; Kamislioglu, M. Photon and neutron shielding performance of boron phosphate glasses for diagnostic radiology facilities. *Results Phys.* **2019**, *12*, 1457–1464. [[CrossRef](#)]
18. Tiamduantawan, P.; Wimolmala, E.; Meesat, R.; Saenboonruang, K. Effects of Sm_2O_3 and Gd_2O_3 in poly (vinyl alcohol) hydrogels for potential use as self-healing thermal neutron shielding materials. *Radiat. Phys. Chem.* **2020**, *172*, 108818. [[CrossRef](#)]
19. Kaewnuam, E.; Wantana, N.; Tanusilp, S.; Kurosaki, K.; Limkitjaroenporn, P.; Kaewkhao, J. The influence of Gd_2O_3 on shielding, thermal and luminescence properties of $\text{WO}_3\text{-Gd}_2\text{O}_3\text{-B}_2\text{O}_3$ glass for radiation shielding and detection material. *Radiat. Phys. Chem.* **2022**, *190*, 109805. [[CrossRef](#)]
20. Gwaily, S.E.; Badawy, M.M.; Hassan, H.H.; Madani, M. Natural rubber composites as thermal neutron radiation shields: I. $\text{B}_4\text{C/NR}$ composites. *Polym. Test.* **2002**, *21*, 129–133. [[CrossRef](#)]
21. Ozdemir, T.; Akbay, I.K.; Uzun, H.; Reyhancan, I.A. Neutron shielding of EPDM rubber with boric acid: Mechanical, thermal properties and neutron absorption tests. *Prog. Nucl. Energy* **2016**, *89*, 102–109. [[CrossRef](#)]
22. El-Khatib, A.M.; Doma, A.S.; Badawi, M.S.; Abu-Rayan, A.E.; Aly, N.S.; Alzahrani, J.S.; Abbas, M.I. Conductive natural and waste rubbers composites-loaded with lead powder as environmental flexible gamma radiation shielding material. *Mater. Res. Express* **2020**, *7*, 105309. [[CrossRef](#)]
23. Xu, C.; Cao, L.; Lin, B.; Liang, X.; Chen, Y. Design of self-healing supramolecular rubbers by introducing ionic cross-links into natural rubber via a controlled vulcanization. *ACS Appl. Mater. Interfaces* **2016**, *8*, 17728–17737. [[CrossRef](#)]

24. Xu, C.; Cao, L.; Huang, X.; Chen, Y.; Lin, B.; Fu, L. Self-healing natural rubber with tailorable mechanical properties based on ionic supramolecular hybrid network. *ACS Appl. Mater. Interfaces* **2017**, *9*, 29363–29373. [[CrossRef](#)] [[PubMed](#)]
25. Norhazariah, S.; Azura, A.R.; Sivakumar, R.; Azahari, B. Effect of different preparation methods on crosslink density and mechanical properties of Carrageenan filled natural rubber (NR) latex films. *Procedia Chem.* **2016**, *19*, 986–992. [[CrossRef](#)]
26. Boden, J.; Bowen, C.R.; Buchard, A.; Davidson, M.G.; Norris, C. Understanding the effects of cross-linking density on the self-healing performance of epoxidized natural rubber and natural rubber. *ACS Omega* **2022**, *7*, 15098–15105. [[CrossRef](#)]
27. Gerward, L.; Guilbert, N.; Bjorn Jensen, K.; Levring, H. X-ray absorption in matter. Reengineering XCOM. *Radiat. Phys. Chem.* **2001**, *60*, 23–24. [[CrossRef](#)]
28. Tiandungtawan, P.; Kamkaew, C.; Kuntonwatchara, S.; Wimolmala, E.; Saenboonruang, K. Comparative mechanical, self-healing, and gamma attenuation properties of PVA hydrogels containing either nano- or micro-sized Bi₂O₃ for use as gamma-shielding materials. *Radiat. Phys. Chem.* **2020**, *177*, 109164. [[CrossRef](#)]
29. Kires, M. Archimedes' principle in action. *Phys. Educ.* **2007**, *42*, 484. [[CrossRef](#)]
30. Moonart, U.; Utara, S. Effect of surface treatments and filler loading on the properties of hemp fiber/natural rubber composites. *Cellulose* **2019**, *26*, 7271–7295. [[CrossRef](#)]
31. Sears, V.F. Neutron scattering lengths and cross sections. *Neutron News* **1992**, *3*, 26–37. [[CrossRef](#)]
32. Piotrowski, T. Neutron shielding evaluation of concretes and mortars: A review. *Const. Build Mater.* **2021**, *277*, 122238. [[CrossRef](#)]
33. Celli, M.; Grazzi, F.; Zoppi, M. A new ceramic material for shielding pulsed neutron scattering instruments. *Nucl. Instrum. Methods Phys. Res. A.* **2006**, *565*, 861–863. [[CrossRef](#)]
34. Xu, Z.G.; Jiang, L.T.; Zhang, Q.; Qiao, J.; Gong, D.; Wu, G.H. The design of a novel neutron shielding B₄C/Al composite containing Gd. *Mater. Des.* **2016**, *111*, 375–381. [[CrossRef](#)]
35. Manohara, S.R.; Hanagodimath, S.M.; Thind, K.S.; Gerward, L. On the effective atomic number and electron density: A comprehensive set of formulas for all types of materials and energies above 1 keV. *Nucl. Instrum. Methods Phys. Res. Sec. B* **2008**, *266*, 3906–3912. [[CrossRef](#)]
36. Singh, V.P.; Badiger, N.M. Study of mass attenuation coefficients, effective atomic numbers and electron densities of carbon steel and stainless steels. *Radioprotection* **2013**, *48*, 431–443. [[CrossRef](#)]
37. Aghaz, A.; Faghihi, R.; Mortazavi, S.M.J.; Haghparast, A.; Mehdizadeh, S.; Sina, S. Radiation attenuation properties of shields containing micro and nano WO₃ in diagnostic X-ray energy range. *Int. J. Radiat. Res.* **2016**, *14*, 127–131. [[CrossRef](#)]
38. Chantler, C.T. Detailed tabulation of atomic form factors, photoelectric absorption and scattering cross section, and mass attenuation coefficients in the vicinity of absorption edges in the soft X-ray (Z=30–36, Z=60–89, E=0.1 keV–10 keV), addressing convergence issues of earlier work. *J. Phys. Chem. Ref. Data* **2000**, *29*, 597.
39. McCaffrey, J.P.; Shen, H.; Downton, B.; Mainegra-Hing, E. Radiation attenuation by lead and nonlead materials used in radiation shielding garments. *Med. Phys.* **2007**, *34*, 530–537. [[CrossRef](#)]
40. Ozdemir, T.; Gungor, A.; Reyhancan, I.A. Flexible neutron shielding composite material of EPDM rubber with boron trioxide: Mechanical, thermal investigations and neutron shielding tests. *Radiat. Phys. Chem.* **2017**, *131*, 7–12. [[CrossRef](#)]
41. Intom, S.; Kalkornsurapranee, E.; Johns, J.; Kaewjaeng, S.; Kothan, S.; Hongtong, W.; Chaiphaksa, W.; Kaewkhao, J. Mechanical and radiation shielding properties of flexible material based on natural rubber/ Bi₂O₃ composites. *Radiat. Phys. Chem.* **2020**, *172*, 108772. [[CrossRef](#)]
42. Kong, S.M.; Mariatti, M.; Busfield, J.J.C. Effects of types of fillers and filler loading on the properties of silicone rubber composites. *J. Reinf. Plast. Compos.* **2011**, *30*, 1087–1096. [[CrossRef](#)]
43. Frohlich, J.; Niedermeier, W.; Luginsland, H.D. The effect of filler–filler and filler–elastomer interaction on rubber reinforcement. *Compos. Part A Appl. Sci. Manuf.* **2005**, *36*, 449–460. [[CrossRef](#)]
44. Sambhudevan, S.; Shankar, B.; Appukuttan, S.; Joseph, K. Evaluation of kinetics and transport mechanism of solvents through natural rubber composites containing organically modified gadolinium oxide. *Plast. Rubber Compos.* **2016**, *45*, 216–223. [[CrossRef](#)]
45. Fan, R.L.; Zhang, Y.; Li, F.; Zhang, Y.X.; Sun, K.; Fan, Y.Z. Effect of high-temperature curing on the crosslink structures and dynamic mechanical properties of gum and N330-filled natural rubber vulcanizates. *Polym. Test.* **2001**, *20*, 925–936. [[CrossRef](#)]
46. Liu, Y.; Li, Z.; Liu, R.; Liang, Z.; Yang, J.; Zhang, R.; Zhou, Z.; Nie, Y. Design of self-healing rubber by introducing ionic interaction to construct a network composed of ionic and covalent cross-linking. *Ind. Eng. Chem. Res.* **2019**, *58*, 14848–14858. [[CrossRef](#)]
47. Zhao, M.; Chen, H.; Yuan, J.; Wu, Y.; Li, S.; Liu, R. The study of ionic and entanglements self-healing behavior of zinc dimethacrylate enhanced natural rubber and natural rubber/butyl rubber composite. *J. Appl. Polym. Sci.* **2022**, *139*, 52048. [[CrossRef](#)]
48. Wu, M.; Yang, L.; Shen, Q.; Zheng, Z.; Xu, C. Endeavour to balance mechanical properties and self-healing of nature rubber by increasing covalent crosslinks via a controlled vulcanization. *Eur. Polym. J.* **2011**, *161*, 110823. [[CrossRef](#)]
49. Peymanfar, R.; Selseleh-Zakerin, E.; Ahmadi, A.; Saeidi, A.; Tavassoli, S.H. Preparation of self-healing hydrogel toward improving electromagnetic interference shielding and energy efficiency. *Sci. Rep.* **2021**, *11*, 16161. [[CrossRef](#)]
50. Park, J.; Kim, M.; Choi, S.; Sun, J. Self-healable soft shield for γ -ray radiation based on polyacrylamide hydrogel composites. *Sci. Rep.* **2020**, *10*, 21689. [[CrossRef](#)]